Coupled, region based level sets for segmentation of the thalamus and its subnuclei in DT-MRI.

Lisa Jonasson, Cecilia Richero Wilson, Xavier Bresson,
Patric Hagmann, Reto Meuli, Jean-Philippe Thiran
Rapport ITS 20.2004

Abstract—

We present a method for segmenting the thalamus and its subnuclei from Diffusion Tensor Magnetic Resonance Images using coupled, region based, level sets in 3D. Each surface, formed from the zero'th level set of the level set function, is associated with the most representative tensor contained within the surface. All neighboring voxels are then assigned to a region by finding the surface which representative tensor is most similar to the actual tensor. From these similarity measures a region based force is defined and the surfaces are dependent on each other through a coupling force[1].

For the segmentation of the thalamus itself, we have used a region based, level set method on the fractional anisotropy maps. In this case the regions have been defined from the histogram by matching Gaussians according to [1]. To improve the segmentation we have coupled the level set evolving in the thalamus with two other level sets segmenting the surrounding structures using information not only from the anisotropy map but also from a map describing the mean diffusion. This segmentation has then been used as a mask for segmenting the subnuclei.

I. Introduction

The thalamus can be considered being the central relay station for nerve impulses in the brain. Axons from every sensory system (except olfaction) synapse here as the last site before the information reaches the cerebral cortex. Information received from diverse brain regions is passed on to the cortex through the thalamus.

Anatomically, it is a large, dual lobed mass made mainly of grey matter cells, located in the center of the brain. Each lobe measures approximately 4 centimeters. It is part of the diencephalon and we find it deep inside the cerebral hemispheres and next to the ventricles. The third ventricle shares its lateral walls with the thalamus, as it separates the two thalamic bodies. These are connected by a piece of thalamic white matter tissue called *massa intermedia*. This is not the only white matter in the thalamus, several fibers also pass through and around it. The thalamus, situated at the top of the brainstem, superior to the hypothalamus, communicates sensory, motor and associative brain regions.

Some parts of the thalamus play a major role in the regulation of consciousness, alertness, arousal, and possibly attention, which partially explains why the thalamus is considered to be part of the limbic system.

The thalamic cytoarchitecture is divided into different clusters, a heterogeneous group of nuclei, each with a specific function. The thalamic nuclei have traditionally been studied with histological methods and their number varies depending on the method used. However most studies identify 14 major nuclei, some of them being subdivided.

The importance of generating an exact map of the thalamus comes from the fact that thalamic changes are involved in a large number of diseases, such as schizophrenia, Parkinson's disease and multiple sclerosis. The thalamic atlases are used to target the pertinent nucleus in presurgical planning of these diseases. However there is a high inter-subject variability in the location and size of the thalamic nuclei and therefore generic thalamic atlases may be highly inaccurate. Resolving thalamic nuclei by noninvasive imaging would be a great step forward as it would enable, among other things, more accurate neurosurgical planning for the diseases mentioned above, giving the possibility of generating a personal thalamic atlas for each patient. Unfortunately current imaging methods such as CT [1] and conventional Magnetic Resonance Imaging(MRI) do not provide the necessary image contrast to differentiate the nuclei so radiological identification of individual thalamic nuclei is not currently possible. [2] have shown how Diffusion Tensor MRI (DT-MRI) can differentiate the principal thalamic nuclei, non-invasively, basing on the characteristic fiber orientation, which is assumed to stay the same all along one certain nucleus and varies from one nucleus to another.

DT-MRI is a new modality that permits non-invasive quantification of the water diffusion in living tissues. The Diffusion Tensor(DT) provides information about the intensity of the water diffusion in any direction at a certain point. The water diffusion in the brain is highly affected by its cellular organization. In particular axonal cell membrane and myelin sheath are the main components restricting water mobility [3]. Hence the measured DT becomes highly anisotropic and oriented in areas of compact nerve fiber organization, providing an indirect way of fiber tract identification.

The DT is normally interpreted by calculating its eigenvalues and eigenvectors, the eigenvector corresponding to the highest eigenvalue describes the direction of the principal diffusion and the eigenvalue is a quantitative measure of the diffusion in that direction.

Today, DT-MRI is mostly used for determining brain connectivity using fiber tractography algorithms [4], [5], [6], [7]. However, more people are now using it for segmentation purposes[8], [9], [10], [11]. In [12] we presented a geometric flow implemented with level set methods for fiber tract segmentation by measuring the diffusive similarity be-

[1] CT: Computerized Tomography

tween voxels. The flow is evolving using this similarity as a front propagation criteria. The front propagation speed in a certain direction is proportional to the similarity between the tensors lying on the surface and their neighbors in that propagation direction. The method is based on the assumption that successive voxels in a tract have similar diffusion properties. [9] also used level set methods to segment tensor fields, they used a distance metric between tensors to define a region based force for front propagation.

The method we propose to segment the thalamus and its subnuclei is a continuation on our work on fiber tract segmentation and has a high resemblance with the work of Wang et al. We use region based, coupled level sets to simultaneously the subnuclei. Each surface, formed from the zero'th level set of the level set function, is associated with the most representative tensor contained within the surface. All neighboring voxels are then assigned to a region by finding the surface which representative tensor is most similar to the actual tensor. From these similarity measures a region based force is defined and the surfaces are dependent on each other through a coupling force[1].

For the segmentation of the thalamus itself, we have used a region based, level set method on the fractional anisotropy maps. In this case the regions have been defined from the histogram by matching Gaussians according to [1]. To improve the segmentation we have coupled the level set evolving in the thalamus with two other level sets segmenting the surrounding structures using information not only from the anisotropy map but also from a map describing the mean diffusion. This segmentation has then been used as a mask for segmenting the subnuclei.

First we will briefly present the concept of diffusion tensors and basic theories on region based front propagation with level set implementation. We will then show how to use similarity measures for diffusion tensors to propagate a surface and how this can be used for white and gray matter segmentation. The validation will be made on synthetic images and we will show segmentation results on real DT-MRI of the brains of two healthy subject.

II. Background Theory

A. Diffusion Tensor Imaging and Tensor Similarity Measures

Diffusion tensor magnetic resonance imaging(DT-MRI) permits in vivo measures of the self-diffusion of water in living tissues. The tissue structure will affect the Brownian motion of the water molecules which will lead to an anisotropic diffusion that is measured by diffusion weighted MRI along at least six independent axes. A normalizing image without diffusion weighting is also required. As a second order approximation, the measured anisotropic motion can be modelled by an anisotropic Gaussian, that can be parameterized by the diffusion tensor in each voxel [13] to create a 3D field of diffusion tensors.

The diffusion tensor is a 3 x 3 symmetric, semi-positive definite matrix. By diagonalizing the DT we obtain the eigenvalues ($\lambda_1, \lambda_2, \lambda_3$ where $\lambda_1 \geq \lambda_2 \geq \lambda_3$) and the corresponding eigenvectors ($\mathbf{e_1}, \mathbf{e_2}, \mathbf{e_3}$). Since the tensor is symmetric and semi-positive definite the eigenvalues will always be non-negative. Although noise can destroy the semi-positivity of the measured DTs. The diffusion tensor can then be described in terms of its eigenvalues and eigenvectors.

$$D = (\mathbf{e_1}\mathbf{e_2}\mathbf{e_3}) \begin{pmatrix} \lambda_1 & 0 & 0 \\ 0 & \lambda_2 & 0 \\ 0 & 0 & \lambda_3 \end{pmatrix} (\mathbf{e_1}\mathbf{e_2}\mathbf{e_3})^{\mathbf{T}}. \quad (1)$$

The largest eigenvalue and its corresponding eigenvector describes the quantity and direction of the principal diffusion.

[14] have been exploring many similarity measures for tensors to perform elastic matching of diffusion tensor images. These measures do not only take the magnitudes of the diffusivity into account but also the directions. The most common similarity measure between two tensors are the tensor scalar product (TSP). This is a measure of the overlap between two tensors:

$$D_1 : D_2 = \text{Trace}(D_1 D_2) = \sum_{j=1}^{3}\sum_{i=1}^{3} \lambda_{1i}\lambda_{2j}(e_{1i}e_{2j})^2. \quad (2)$$

The TSP is often normalized to avoid influence of the relative size of the two tensors. This will emphasize the shape and orientation of the tensor.

$$\text{NTSP}(D_1, D_2) = \frac{D_1 : D_2}{\text{Trace}(D_1)\text{Trace}(D_2)}. \quad (3)$$

Another way of measuring the tensor similarity using the full tensor information that is also presented by Alexander and it is the tensor difference (TD).

$$\text{TD}(D_1, D_2) = \sqrt{(D_1 - D_2) : (D_1 - D_2)} \quad (4)$$

where . : . is given as in (2). The TD measures the difference in size and shape as well as orientation between the two tensors.

The diffusion in a certain direction, $\hat{x}$, is given by the the double contraction of the DT with the vector:

$$d(\hat{x}) = \hat{x} D \hat{x}. \quad (5)$$

A way of directly comparing the diffusion between two tensors is to compare the diffusion in the direction of all unit vectors on a sphere, $\hat{x}$, using the double contraction. We will call this similarity measure for integral similarity (IS).

$$\text{IS}(D_1, D_2) = \int \min\left(\frac{d_1(\hat{x})}{d_2(\hat{x})}, \frac{d_2(\hat{x})}{d_1(\hat{x})}\right) d\hat{x}, \quad (6)$$

where $d_1(\hat{x})$ is the diffusion in direction $\hat{x}$ for the diffusion tensor D_1. The IS gives us a percentage of the common diffusion for the two tensors.

To find the most representative tensor data set, [15] uses a distance metric between two tensors, (A, B):

$$d(A, B) := \sqrt{(A - B) : (A - B)}, \quad (7)$$

which in expanded form becomes:

$$\begin{aligned} d(A,B)^2 :=& (A_{11}-B_{11})^2 + (A_{22}-B_{22})^2 \\ &+ (A_{33}-B_{33})^2 + 2(A_{12}-B_{12})^2 \\ &+ 2(A_{13}-B_{13})^2 + 2(A_{23}-B_{23})^2. \end{aligned} \quad (8)$$

A similar distance metric between a pair of images, i and j is then defined as:

$$d_{ij} = \sqrt{\sum_{\text{all voxels}} d(D_i, D_j)^2}. \quad (9)$$

The root means square distance between a tensor in a voxel in the i'th image and the corresponding voxel in the other data set becomes:

$$c_i = \frac{\sqrt{\sum_{i=1,j\neq i}^{n} d_{ij}^2}}{n-1}. \quad (10)$$

The most representative data set is then the data set with the lowest value of c_i.

B. Geometrical Flows and Level Set Implementation

Geometrical flows and especially curvature- or curve shortening flows are becoming more and more important tools in computer vision. A curvature flow is a curve or surface that evolves at each point along the normal with the velocity depending on the curvature at that point. This process leads to a smoothing of the curves or surfaces to eliminate the effects of noise. The theory is well developed for the two dimensional case and even though some of the properties of the 2D curves, such as the property of shrinking to a point under curvature flow, do not hold in the 3D case, the main part of the theories remains valid and works well for segmentation of 3D objects.

To use the geometrical flows for image segmentation, the evolution of the curve or surface has to depend on external properties determined by the image features. A classical speed function to segment gray scale images is based on the gradient of the images and goes to zero when the surface approaches an edge [16].

A general flow for a 3D closed surface can be described as:

$$\frac{\partial S}{\partial t} = (F+\kappa)\overrightarrow{N}, \quad (11)$$

where F is an image based speed function, κ is an intrinsic speed dependent on the curvature of the surface, S is the surface, $\overrightarrow{N}$ is the surface and t is the time.

To solve this time dependent PDE we use the level set method, introduced by [17], where the evolving surface is considered as a constant level set of a function of a higher dimension. By doing this we obtain a numerically stable algorithm that easily handles topology changes of the evolving surface. In our case the function of higher dimension is the signed distance function, $\phi(t)$, of the evolving surface. This makes the evolution of the zero level set coincide with the evolution of $S(t)$. Thus, the evolution of the signed distance function is described by:

$$\frac{\partial \phi}{\partial t} = (F+\kappa) \mid \nabla \phi \mid . \quad (12)$$

B.1 Geodesic Active Regions and their Statistics

The Geodesic Active Region model was first introduced by [1]. The model consists on segmenting an image into different regions by calculating the probability of every intensity value in the image of being in each region. The key hypothesis that is made to perform segmentation relies on the fact that the image is composed of homogeneous regions. Hence, the intensity properties of a given region can be determined using a Gaussian distribution. The regions are determined from the histogram by fitting Gaussians according to the Maximum Likelihood Principle.

Let I be the input image and *H(I)* its observed density function (histogram). Considering a partition of the image into N non-overlapping regions, let $\{R_i : i \in [1,N]\}$ be the regions and $\{\partial R_i : i \in [1,N]\}$ be the region boundaries.

Let $p(.)$ be the probability density function with respect to the intensity space of the image. Assuming that this probability density function is homogeneous, then an intensity value x is derived by selecting a component k with *o*n a priori *p*robability P_k and then selecting this value according to the distribution of this element $p_k()$. This hypothesis leads to a mixture model of Gaussian elements:

$$p(x) = \sum P_k p_k(x) \quad (13)$$

$$p_k(x) = \frac{1}{\sqrt{2\Pi}\sigma_k} e^{-\frac{(x-\mu_k)^2}{2\sigma_k^2}} \quad (14)$$

where *o*n k *c*orresponds to one of the regions, R_i

The region-based force aims at moving the curve towards the direction that maximizes the *a posteriori* default segmentation probability. The boundary-based force aims at shrinking the curve towards the region boundaries constrained by the curvature.

The region-based term, that will propagate the surfaces, will be proportional to:

$$-\alpha \log\left[\frac{p_i(I(s))}{p_j(I(s))}\right] \quad (15)$$

where $p_i(I(s))$ is the intensity probability density function followed by region R_i. It is therefore the Gaussian distribution that determines the probability of the intensity value corresponding to voxel s, of being in region R_i. Using this function we obtain that when voxel s in effect, belongs to region R_i, then:

$$\begin{aligned} &p_i(I(s)) > p_j(I(s)) \Rightarrow \\ &\frac{p_i(I(s))}{p_j(I(s))} > 1 \Rightarrow -\alpha \log\left[\frac{p_i(I(s))}{p_j(I(s))}\right] < 0 \end{aligned} \quad (16)$$

and so, the speed term is negative and aims at expanding the curve.

If, on the contrary, the voxel s doesn't belong to R_i, then:

$$p_i\left(I\left(s\right)\right) < p_j\left(I\left(s\right)\right) \Rightarrow \\ \frac{p_i\left(I\left(s\right)\right)}{p_j\left(I\left(s\right)\right)} < 1 \Rightarrow -\alpha \log\left[\frac{p_i\left(I\left(s\right)\right)}{p_j\left(I\left(s\right)\right)}\right] > 0 \tag{17}$$

and therefore the speed is positive and the force is applied to shrink the curve, so that voxel s can be attributed to another region.

III. Method

A. Segmentation of the thalamus

The segmentation of the thalamus is made directly from the fractional anisotropy images. The histogram of the fractional anisotropy map is approximated by a mixture of Gaussians. The Gaussians form the probability as described in (13) and the region force is then determined according to (15).

To improve the segmentation we have coupled the level sets with other level sets aiming to segment adjacent structures. The thalamus itself can sometimes be hard to distinguish on just one set of images. However, it is surrounded by structures such as fiber tracts and the cerebrospinal fluid (CSF) that are highly visible in fractional anisotropy maps and mean diffusion maps respectively. Thus, we have evolved three surfaces simultaneously. One for segmenting the fibers in the FA-maps, one for segmenting the CSF in the mean diffusion maps and the third and last one in the thalamus itself. Since all surfaces are not evolving using the same image data the surfaces are only dependent on each other through an artificial coupling force described later in this chapter.

B. Segmentation of the thalamic subnuclei

We have developed a method for gray matter segmentation using tensor similarity measure to identify regions. First the most representative tensor [15] is associated to each evolving surface and every voxel is then associated to a region by calculating the similarity between the tensor in that voxel and the average tensor of the different regions. A recently published paper is also based on a similar region force as we are using but are not using coupled level sets [9].

In our case the region force will look like:

$$F_i = -\log\left(\frac{\mathrm{IS}(\mathbf{D}, \mathbf{D_{typ,i}})}{max(\mathrm{IS}(\mathbf{D}, \mathbf{D_{typ,j\neq i}}))}\right), \tag{18}$$

where IS is the integral similarity described in (6). $\mathbf{D_{typ}}$ is the most representative tensor associated with the level set, ϕ_i and is computed according to (10). It is continuously recalculated as the surface is evolving and thereby contains a new set of tensors. F_i will be growing the surface, S_i, in the direction were the diffusion in the voxels are more similar to the tensor that best describes the tensor set lying inside S_i than the typical tensors of the other surfaces, $S_{j\neq i}$. If the similarity is smaller and the voxel is thereby more likely to belong to another region the surface will shrink.

C. Coupling Forces

When propagating several curves, the overlapping between some of them is almost inevitable. When that occurs, it means that a voxel has been initially attributed to two different regions. This is an undesired situation and a constraint to solve or avoid it from the beginning has to be applied. This is done by adding an artificial force in the direction of the normal, to the corresponding level set motion equations. The force will penalize voxels which have been attributed to more than one region. And if necessary, also those voxels which haven't been labelled yet (which don't yet belong to a region).

Inspired by Paragios and Deriche [1], our coupling forces for a given voxel s and a region i, are given by:

$$\sum_{j\in[1,\mathbb{N}]} H_i\left(i, \phi_j\left(s\right)\right) \left|\nabla\phi_i\left(s\right)\right| \tag{19}$$

where the function $H_i\left(,\phi\left(\right)\right)$ is:

$$H_i\left(m, \phi_n\left(s\right)\right) = \begin{cases} 0, & if\ m = i \\ -sign\left(\phi_j\left(s\right)\right), & if\ m \neq i \end{cases}$$

Analyzing the force added, we see it can have two possible effects. The first one is expanding the corresponding curve. If the voxel hasn't yet been attributed to any region, the new force is negative and helps region R_i to expand, occupying the given voxel. The other effect is the shrinking of the curve. If the voxel has been attributed both to region R_i and to some other region R_k then the force will be positive and aim at shrinking region R_i so that overlapping is avoided and voxel s default ends up belonging to just one region.

However, the function presented above, which defines the coupling force, presents some problems. To start with, it penalizes the non-attributed voxels in the same way as the ones attributed to more than one region. Another problem is that the function is not continuous and that may create stability problems during the level sets evolution.

To achieve a more suitable coupling function, we should consider two more properties for it. The first one is the fact that, when a voxel is already attributed to a region j and it is far away from that region's boundaries, the evolution of the level set $\phi_i\left(\right)$ (being R_i another region) should be discouraged to include that voxel in R_i. The second one is that a certain overlapping between two neighbor regions should be tolerated for voxels inside a region which stand very close to its boundaries.

For that purposes, we define the following function:

$$H_a\left(x\right) = -\begin{cases} +1, & if\ x > a \\ -1 & if\ x < -a \\ \frac{1}{\tan(1)}\tan\left(x/a\right), & if\ \ |x| \leq a \end{cases}$$

which will be the basis of the coupling force, defined as:

$$H_i\left(j,\phi_j\left(s\right)\right)=\begin{cases}0, & if\ j=i\\ H_a\left(\phi_j\left(s\right)\right), & if\ j\neq i\ and\\ & \phi_j\left(s\right)\leq 0\\ \frac{1}{N-1}H_a\left(\phi_j\left(s\right)\right), & if\ j\neq i\ and\\ & \left[\cap_{\{k=1,k\neq i\}}^{N}\phi_k\left(s\right)>0\right]\end{cases}$$

The result of introducing this coupling force is that, considering a voxel s and a level set function $\phi_i\left(\right)$, if the voxel is already belonging to another region R_j, then $\phi_j\left(\right)\leq 0$, and the coupling force will be positive, so it will have a shrinking effect, proportional to the distance of the voxel to the boundaries of R_j

$$H_i\left(j,\phi_j\left(s\right)\right)=\begin{cases}+1, & if\ x<-a\\ -\frac{1}{\tan(1)}\tan\left(x/a\right), & if\ \ |x|\leq a\end{cases}$$

On the other hand, if the voxel is not attributed to any region we will find:

$$\phi_j\left(s\right)\geq 0\Rightarrow H_i\left(j,\phi_j\left(s\right)\right)=\frac{1}{N-1}H_a\left(\phi_j\left(s\right)\right)$$

and therefore:

$$H_i\left(j,\phi_j\left(s\right)\right)=\frac{1}{N-1}\begin{cases}+1, & if\ x>a\\ -\frac{1}{\tan(1)}\tan\left(x/a\right), & if\ \ |x|\leq a\end{cases}\tag{20}$$

This force also allows the overlapping when the curves are on top of the real region boundaries.

D. Regularization

As described in II-B, the geometric flows are derived from the theory on curvature flows which leads to a self-regularization of the evolving surfaces. Since DT-MRI contains a high level of noise including this curvature based speed function will be useful for smoothing our result. Since we are mainly looking for spherically shaped objects we use the mean curvature [18].

E. Final evolution

Each one of our surfaces, i, are now evolving according to:

$$\frac{\partial S_i}{\partial t}=(F_i+\kappa_i+H_i)\overrightarrow{N}\tag{21}$$

where F_i is the regions based force (18), κ_i is the mean curvature and H_i is the coupling force (20). This can easily be implemented with the level set method according to the above theories.

IV. Parameters and Implementation Details

The method has been implemented in Matlab 6.1 (The MathWorks, Inc.) except for the reinitialization of the signed distance function, which has been implemented in C and compiled with the mex-library, so the function can be called from Matlab.

A. Preserving the Signed Distance Function

As mentioned in Sec. II-B the evolving surface is considered as the zero level set of its signed distance function (SDF). Due to local dependence of the propagation speed the evolution of the other level sets differs from the zero level set. This creates irregularities that will deform the SDF so it ceases to be a signed distance function. A correct signed distance function is crucial to get a correct and smooth evolution of the surface, since the calculation of the normals and curvatures is directly dependent on the signed distance function. Therefore, a reinitialization of the signed distance map is made at every iteration. It is implemented using the fast marching method to solve the time dependent partial differential equation (PDE) [19]:

$$\frac{\partial\phi}{\partial t}=\text{sign}(\phi_0)(1-\mid\nabla\phi\mid).\tag{22}$$

During the evolution process it is very important to preserve the SDF to assure a correct computation of the normals and the minimal principal curvature. If we do not reinitialize the level set function the propagation will quickly become unstable. Nevertheless, reinitialization is not sufficient to maintain the SDF. Closest to the zero level set we will easily get discontinuities since the speed function can vary a lot between two adjacent voxels. It is also in this area that a correct SDF is of most importance, since the exact position of the zero level set is dependent on the values of the surrounding voxels. To assure the maintenance of the SDF, the speed is calculated only on the zero level set and is then transferred in the direction of the normal to the voxels lying just next to the zero level set.

B. Weighting the Speed Terms

The diffusion dependent and the curvature dependent speed is not always of the same order. To have a satisfactory regularization without inhibiting the front propagation it is therefore important to set the weighting factor between them correctly. The region based term in (21) is then referred to as αF_i, the curvature term to $\beta\kappa\overrightarrow{N}$ and the coupling force to γH_i,

$$\frac{\partial S_i}{\partial t}=(\alpha F_i+\beta\kappa_i+\gamma H_i)\overrightarrow{N},\tag{23}$$

where α, β, γ are weighting parameters.

Finally, the level set function has the following evolution:

$$\frac{\partial\Phi_i}{\partial t}=(\alpha F_i+\beta\kappa_i+\gamma H_i)\mid\nabla\Phi_i\mid\tag{24}$$

For the segmentation of the thalamus when there is no coupling force the weights are set to $\alpha=0.2$, $\beta=10$ and $\gamma=1$.

For segmentation of the subnuclei the parameters are set to $\alpha=5$, $\beta=1$ and $\gamma=1$. The big difference between the parameters in the two cases are due to the different character of the region based force.

C. Coupling force parameter

The coupling force described in (20) is dependent on the parameter a. The choice of a will influence the development of the level set. A small a will have an abrupt transition between the forces and a creates a certain instability of the level sets. A higher value of a does not give this undesired effect but on the other hand allows for a higher distance between the level sets. We have chosen $a = 0.1$. This is a small a that will create instabilities in the level sets when two surfaces becomes very close but since a larger a does not force the level sets to come sufficiently close we have preferred this inconvenience before stability.

D. Determining the regions from the histogram.

To determine the regions from the scalar maps we have used a mixture of Gaussians according to [1]. The Gaussians are fitted using the Maximum Expectation algorithm. The number of Gaussians used is set manually and we have determined the number of Gaussians experimentally by seeing what best segments the thalamus. The fractional anisotropy map has been divided into five regions of which two, represented by the third and fourth Gaussian, corresponds to values that can be seen in the thalamus and one, the fifth Gaussian, to the fibers, see Fig. 1. The mean diffusion map has been divided into four regions of which two, third and fourth, corresponds to the cerebrospinal fluid, see Fig. 1.

V. Validation and results

A. Segmentation of the thalamus

The thalamus has been segmented on three different patients. The results for one of the patients can be seen in Fig. 2 and 3. In Fig. 2 cuts of the three surfaces are displayed on the same image. The surface displayed in green has been segmenting the fibrous regions from the images of fractional anisotropy. The surface displayed in blue has evolved in the image showing the mean diffusion and has segmented the cortico-spinal fluid. The last surface, displayed in red, has evolved in the same map of fractional anisotropy as the surface for segmenting the fibrous region. The surface is dependent on the other surfaces and no overlap between the three surfaces is allowed. Fig. 3 is showing the segmentation result in different cuts.

B. Segmentation of the subthalamic nuclei

B.1 Synthetic data

To validate our method we have created a synthetic tensor volume containing regions of tensors with different properties. To not chose a case too 'easy' we have taken values from different regions of the thalamus. We have used the following tensors:

$$D_1 = 1.0e-003 * \begin{pmatrix} 0.2843 & 0.0377 & 0.0257 \\ 0.2843 & 0.0377 & 0.0257 \\ 0.0257 & -0.0140 & 0.3172 \end{pmatrix}$$

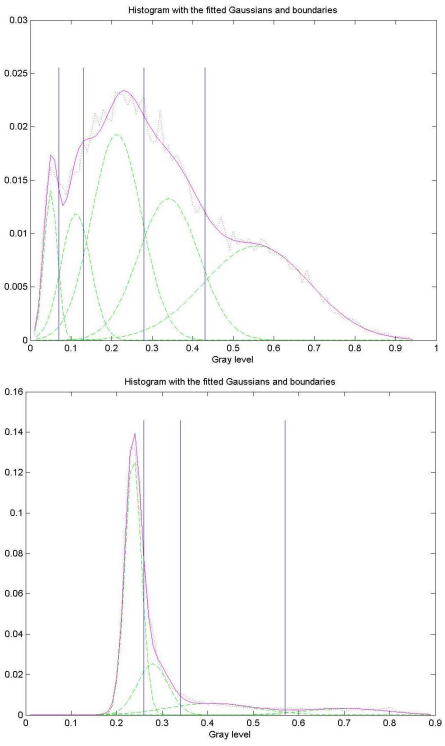

Fig. 1. Histograms estimated with a mixture of Gaussians using the maximum expectation algorithm. Left: Histogram and estimated Gaussians for the fractional anisotropy. The third and fourth Gaussian corresponds to values inside the thalamus och the fifth to fiber values. Right: Histogram and estimated Gaussians for the mean diffusion. The third and fourth Gaussian corresponds to the corticospinal fluid.

$$D_3 = 1.0e-003 * \begin{pmatrix} 0.3231 & 0.0227 & 0.0658 \\ 0.0227 & 0.3106 & 0.0485 \\ 0.0658 & 0.0485 & 0.3128 \end{pmatrix}$$

$$D_5 = 1.0e-003 * \begin{pmatrix} 0.2892 & -0.0019 & 0.0455 \\ -0.0019 & 0.4634 & 0.0398 \\ 0.0455 & 0.0398 & 0.3242 \end{pmatrix}$$

$$D_6 = 1.0e-003 * \begin{pmatrix} 0.3117 & 0.0120 & 0.0734 \\ 0.0120 & 0.2713 & 0.0156 \\ 0.0734 & 0.0156 & 0.3307 \end{pmatrix}$$

$$D_7 = 1.0e-003 * \begin{pmatrix} 0.4061 & -0.0144 & 0.0390 \\ -0.0144 & 0.3682 & 0.0484 \\ 0.0390 & 0.0484 & 0.3097 \end{pmatrix}$$

$$D_8 = 1.0e-003 * \begin{pmatrix} 0.4421 & 0.0166 & 0.0429 \\ 0.0166 & 0.2835 & 0.0260 \\ 0.0429 & 0.0260 & 0.3551 \end{pmatrix}$$

These tensors was then placed in six regions in a 3D volume and rician noise was added [20]. A cut of a slice through the regions can be seen in Fig 4. To initialize the surfaces we ran a k-means clustering algorithm as in [2] and the center points of the obtained clusters were then used as initialization points.

The algorithm was then turning on the tensors fields with three different levels of signal-to-noise-ratio, 32, 16 and 8. Since the tensors are so similar from the beginning the

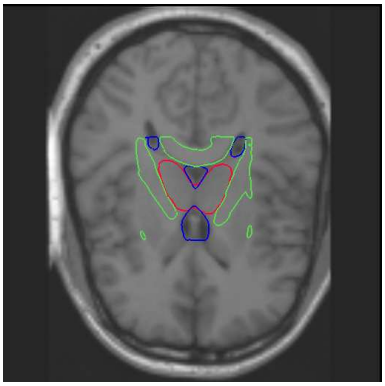

Fig. 2. The segmentation of the thalamus on DT-MRI from a real brain. The three surfaces correspond to the fiber regions, csf and thalamus. The thalamus is surrounded by the fibers and csf.

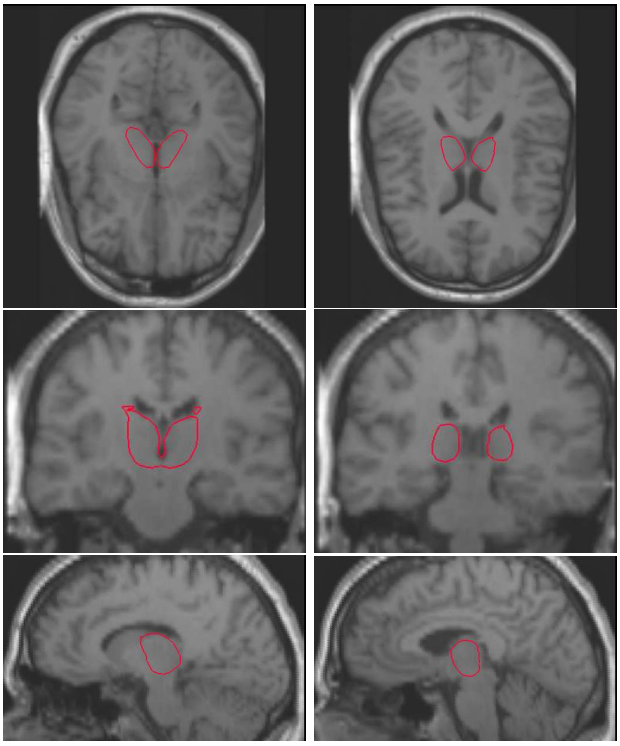

Fig. 3. The segmentation of the thalamus on DT-MRI from a real brain.

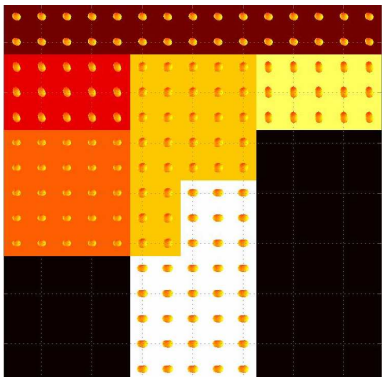

Fig. 4. A cut of the synthetic tensor field used to test the segmentation method.

noise is very disturbing and with an SNR of 8 it is almost impossible to distinguish the difference between the regions so finally we decided to not use this.

In Fig. 5 the regions have been segmented on the synthetic tensor field without any noise added. The results is shown on the result from the k-means algorithm. We see that our method manages better to segment the regions that are more elongated. The k-means clustering algorithm weights the distance between the tensors as well as the similarity between them and when they are far apart they get more easily attributed to an other region. If the algorithm puts more weight to the similarity than the spacial distance the clusters becomes less centered and non-connected clusters can appear. In Fig. 6 the same segmentations have been made on a field with a SNR = 32.

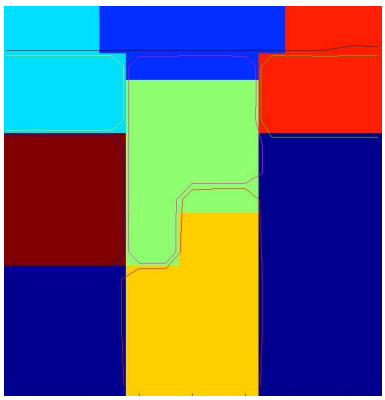

Fig. 5. The segmentation result on a synthetic field, without any noise added, for the coupled, level set algorithm displayed on the segmentation result obtained with the k-means algorithm. The level set methods results in a better segmentation for elongated structures.

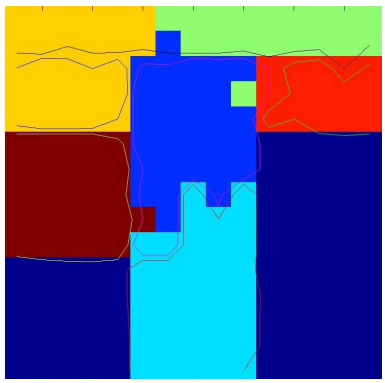

Fig. 6. The segmentation result on a synthetic field, with SNR=32, for the coupled, level set algorithm displayed on the segmentation result obtained with the k-means algorithm. The level set methods results in a better segmentation for elongated structures.

B.2 Real DT-MRI

The method has been tested on three persons. The results can be seen in Fig.7, 8 and 9. The resulting surfaces are shown in 3D and as 2D contours on fractional anisotropy maps. The color of the surfaces are determined

from the direction of principal diffusion of the most representative tensor inside the surface.

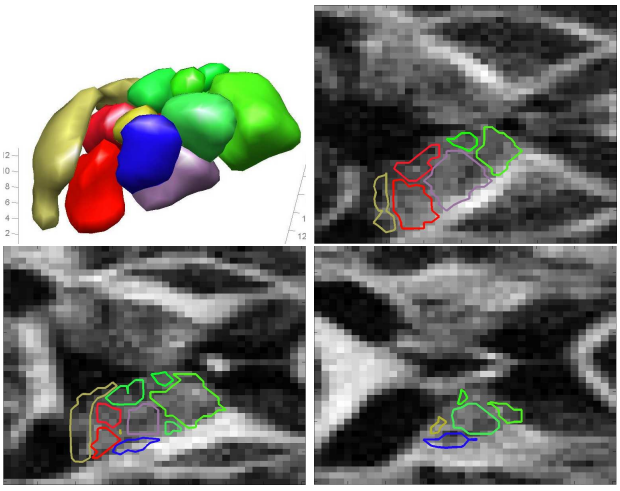

Fig. 7. The segmentation of subthalamic nuclei on DT-MRI from a real brain.

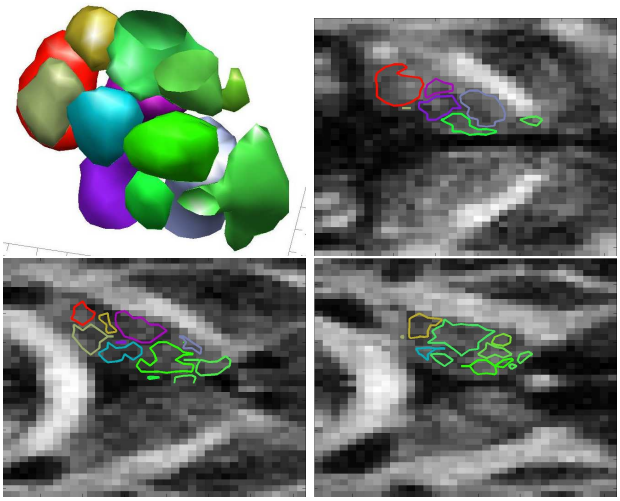

Fig. 8. The segmentation of subthalamic nuclei on DT-MRI from a real brain.

VI. Discussion and Conclusion

We have presented a new method for segmenting the thalamic region and the thalamic subnuclei by defining a region based force from the diffusive similarity. The method manages to perform a segmentation based on the similarity between the diffusive properties of the voxels. The results on real DT-MRI from human brains have been compared with results from a k-means clustering algorithm.

To further validate the work the results will be compared with anatomical brain atlases by an expert.

We will continue the work trying to find the best way of initializing the surfaces, both concerning position and number of surfaces.

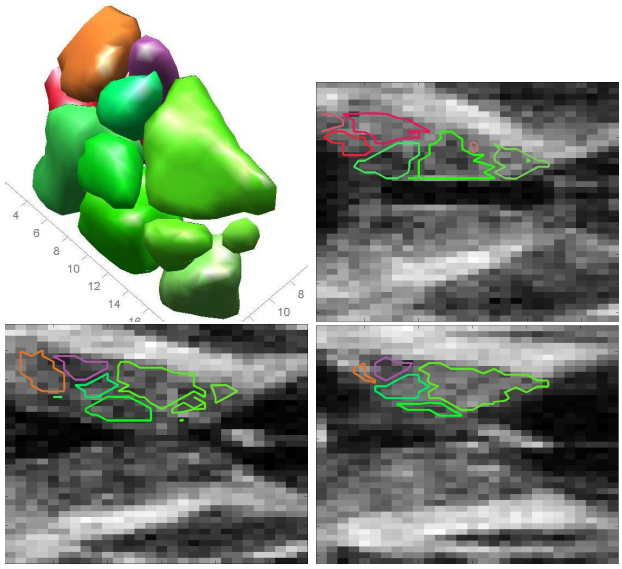

Fig. 9. The segmentation of subthalamic nuclei on DT-MRI from a real brain.

Acknowledgements

This work is supported by the Swiss National Science Foundation grant number 2153-066943.01.

References

[1] N. Paragios and R. Deriche, "Coupled geodesic active regions for image segmentation," Tech. Rep. 3783, INRIA, Oct. 1999.

[2] M. R. Wiegell, D. S. Tuch, H. B.W. Larsson, and V. J. Wedeen, "Automatic segentation of thalamic nuclei from diffusion tensor magnetic resonance imaging," *NeuroImage*, vol. 19, pp. 391–401, 2003.

[3] C. Beaulieu, "The basis of anisotropic water diffusion in the nervous system - a technical review.," *NMR in Biomedicine*, vol. 15, no. 7-8, pp. 435–455, 2002.

[4] P. Hagmann, J.P. Thiran, L. Jonasson, P. Vandergheynst, S. Clarke, and R. Meuli, "Dti mapping of human brain connectivity: Statistical fibre tracking and virtual dissection," *NeuroImage*, vol. 19, no. 3, pp. 545–554, 2003.

[5] T.E. Conturo, N.F. Lori, T.S. Cull, E. Akbudak, A.Z. Snyder, J.S. Shimony, R.C. McKinstry, H. Burton, and M.E. Raichle, "Tracking neuronal fiber pathways in the living human brain," *Proc Natl Acad Sci U S A*, vol. 96, no. 18, pp. 10422–7, 1999.

[6] BC. Vemuri, Rao M. Chen, Y., T. McGraw, Z. Wang, and T. Mareci, "Fiber tract mapping from diffusion tensor mri.," in *Proceedings of the IEEE Workshop on Variational and Level Set Methods in Computer Vision*, 2001, pp. 81–88.

[7] P.J. Basser, S. Pajevic, C. Pierpaoli, J. Duda, and A. Aldroubi, "In vivo fiber tractography using dt-mri data," *Magn Reson Med*, vol. 44, no. 4, pp. 625–32, 2000.

[8] L. Zhukov, K. Museth, D. Breen, R. Whitaker, and A. Barr, "Level set modelling and segmentation of dt-mri brain data.," *Journal of Electronic Imaging*, vol. 12, no. 1, pp. 125–133, 2003.

[9] Z. Wang and B. Vemuri, "Tensor field segmentation using region based active contour model," in *ECCV 2004, LNCS 3024*. 2004, pp. 304–315, Springer.

[10] C. Feddern, J. Weickert, and B. Burgeth, "Level-set methods for tensor valued images," in *Proc. Second IEEE Workshop on Variational, Geometric and Level Set Methods in Computer Vision.*, 2003, pp. 65–72.

[11] M. Rousson, C. Lenglet, and R. Deriche, "Level set and region based surface propagation for diffusion tensor mri segmentation," in *CVAMIA and MMBIA*, 2004.

[12] L. Jonasson, P. Hagmann, X. Bresson, R. Meuli, O. Cuisenaire, and J.-Ph. Thiran, "White matter mapping in dt-mri using geometric flows.," in *Computer Aided Systems Theory - Eurocast 2003, LNCS 2809*. 2003, pp. 585–595, Springer.

[13] P.J. Basser, J. Mattiello, and D. Le Bihan, "Mr diffusion tensor spectography and imaging," *Biophys. J.*, vol. 66, pp. 259–267, 1994.

[14] D. Alexander, J. Gee, and R. Bajcsy, "Similarity measures for matching diffusion tensor images," in *Proceedings BMCV'99*, 1999.

[15] D.K. Jones, L.D. Griffin, D.C. Alexander, M. Catani, , M.A. Horsfield, R. Howard, and S.C. Williams, "Spatial normalization and averaging of diffusion tensor mri data sets," *NeuroImage*, vol. 17, pp. 592–617, 2002.

[16] V. Caselles, R. Kimmel, and G. Sapiro, "Geodesic active contours," *International Journal of Computer Vision*, vol. 22, pp. 61–79, 1997.

[17] S. Osher and J.A. Sethian, "Fronts propagating with curvature-dependent speed: Algorithms based on Hamilton-Jacobi formulations," *Journal of Computational Physics*, vol. 79, pp. 12–49, 1988.

[18] JA. Sethian, *Level set methods and fast marching methods: Evolving interfaces in computational geometry, fluid mechanics, computer vision, and materials science*, 1999.

[19] M. Sussman and E. Fatemi, "An efficient, interface preserving level set re-distancing algorithm and its application to incompressible fluid flow," *SIAM Journal on Scientific Computing*, vol. 20, no. 4, pp. 1165–1191, 1999.

[20] J.D. Tournier, F. Calamante, M.D. King, D.G. Gadian, and A. Connelly, "Limitations and requirements of diffusion tensor fiber tracking: an assessment using simulations," *Magn Reson Med*, vol. 47, no. 4, pp. 701–8, 2002.